Available online at www.sciencedirect.com
SCIENCE DIRECT®
Journal of Solid State Chemistry 175 (2003) 116–123
JOURNAL OF SOLID STATE CHEMISTRY
http://elsevier.com/locate/jssc

Bond-length fluctuations in transition-metal oxoperovskites

J.B. Goodenough,* J.-S. Zhou, F. Rivadulla, and E. Winkler

Texas Materials Institute, University of Texas at Austin, M/C C2201 Austin, TX 78712-1063, USA

Received 25 August 2002; accepted 15 December 2002

Abstract

Bond-length fluctuations in transition-metal oxoperovskites may give rise to two-phase fluctuations in what appears to be a single phase to a diffraction experiment. Orbital disorder at Jahn–Teller ions results in bond-length fluctuations that give 3D-ferromagnetic, vibronic Mn(III)–O–Mn(III) superexchange interactions and allow disproportionation into Mn(IV) and Mn(II) in $LaMnO_3$; where orbitally ordered and disordered phases coexist, an external magnetic field stabilizes the orbitally disordered, ferromagnetic phase relative to the orbitally ordered, antiferromagnetic phase. Spin–lattice interactions in the paramagnetic phase of charge-transfer compounds give bond-length fluctuations arising from the semicovalent component of the superexchange interactions. At the crossover from localized to itinerant electronic behavior, the coexistence of two-phase fluctuations has been demonstrated in both the single-valent $RNiO_3$ family (R = rare-earth, A = alkaline-earth) and the mixed-valent $R_{0.5}A_{0.5}MnO_3$ perovskites. "Bad-metal" behavior is found to be associated with bond-length fluctuations.

Keywords: Perovskites; Jahn–Teller deformations, Dynamic; Spinodal phase segregation; Spin–lattice interactions; Vibronic properties; Bad metals

1. Introduction

Bond-length fluctuations may give anomalously large Debye–Waller factors, but they are not otherwise detected by a conventional diffraction experiment. However, they can be detected directly by fast experimental probes, and they may be inferred indirectly from several unusual physical properties that they impart to a crystalline solid. In this paper, we review some examples of bond-length fluctuations in oxoperovskites that result from orbital fluctuations at Jahn–Teller ions, from spin–lattice coupling in paramagnetic charge-transfer oxides, and from phase fluctuations at a crossover from localized to itinerant electronic behavior in both a single-valent and a mixed-valent system.

1.1. The geometric tolerance factor

In the AMO_3 perovskite structure, the tolerance factor

$$t \equiv (A-\mathrm{O})/\sqrt{2}(M-\mathrm{O}) \tag{1}$$

is a measure of the mismatch between the equilibrium (A–O) and (M–O) bond lengths. A $t<1$ is accommodated by a cooperative rotation of the $MO_{6/2}$ octahedra about a [001], a [111] or a [110] axis to give tetragonal, rhombohedral, or orthorhombic symmetry. The equilibrium (A–O) and (M–O) bond lengths are calculated from the sums of tabulated ionic radii determined empirically from ambient X-ray data. In a transition-metal perovskite, the thermal expansion of the (A–O) bond is normally greater than that of the (M–O) bond, which makes $\mathrm{d}t/\mathrm{d}T>0$; the compressibility of the (A–O) bond is normally greater than that of the (M–O) bond to give $\mathrm{d}t/\mathrm{d}P<0$, but at the crossover from localized to itinerant electronic behavior in the MO_3 array, a double-well potential for the equilibrium (M–O) bond length gives the $\langle(M\text{–O})\rangle$ bond a larger compressibility and, therefore, a $\mathrm{d}t/\mathrm{d}P>0$.

1.2. The virial theorem of quantum mechanics

The origin of the double-well potential at the crossover from localized to itinerant electronic behavior is most easily understood from the virial theorem, which states that for a system of particles in central force fields,

$$2\langle T\rangle + \langle V\rangle = 0, \tag{2}$$

*Corresponding author.
E-mail address: jgoodenough@mail.utexas.edu (J.B. Goodenough).

0022-4596/03/$ - see front matter © 2003 Elsevier Science (USA). All rights reserved.
doi:10.1016/S0022-4596(03)00041-0

where the mean kinetic energy $\langle T \rangle$ for electrons decreases as the volume the electrons occupy increases. Since the electrons of a crystal are bound, their mean potential energy is $\langle V \rangle < 0$. At a transition from localized to itinerant electrons, the volume occupied by an electron increases discontinuously, and the resulting discontinuous $\Delta \langle T \rangle < 0$ requires, from the virial theorem, a discontinuous $\Delta |\langle V \rangle| < 0$. Consequently, there is a discontinuous change in the (M–O) bond length, which makes the transition first- order. Where phase segregation would occur at too low a temperature for atomic diffusion, a spinodal phase segregation is made possible in an oxoperovskite by cooperative oxide-ion displacements. Since the transition-metal d electrons are antibonding with respect to an M–O bond, a $\Delta |\langle V \rangle| < 0$ is accomplished by a decrease in the (M–O) bond length, so

$$(M-\mathrm{O})_{\mathrm{localized}} > (M-\mathrm{O})_{\mathrm{itinerant}}. \quad (3)$$

In an orthorhombic or rhombohedral perovskite, the $(180^\circ - \phi)$ M–O–M bond angles are less than 180°. Therefore, the (M–O) bond lengths within an itinerant-electron phase may be shortened by an O^{2-}-ion displacement perpendicular to the bond axis; and at the interface between localized and itinerant phases, a displacement along the bond axis makes a short (M–O) bond on one side and a long (M–O) bond on the other. These cooperative oxide-ion displacements may fluctuate or they may become long-range ordered into a charge-density wave.

2. Single-valent oxoperovskites containing Mn(III)

2.1. $LnMnO_3$

The localized high-spin Mn(III) t^3e^1 configurations in $LaMnO_3$ have a twofold e-orbital degeneracy that may be removed by a Jahn–Teller deformation of the $MnO_{6/2}$ octahedra to tetragonal or orthorhombic symmetry. Below 750 K, a cooperative Jahn–Teller deformation creates in the (001) planes two short and two long Mn–O bonds at each Mn(III) ion; on traversing a [100] or [010] axis, the Mn–O bond lengths alternate:–short–short–long–long–short–; the O^{2-} ions remain at the center of a c-axis Mn–O–Mn bond with medium length. This cooperative orbital ordering is superimposed on the O-orthorhombic structure ($c/a > \sqrt{2}$ in $Pbnm$) to give an O′-orthorhombic structure with $c/a < \sqrt{2}$. Below a Neél temperature $T_N \approx 140$ K, the e^1 O-e^0 interactions in the (001) planes are ferromagnetic and the c-axis t^3-O-t^3 interactions couple the ferromagnetic (001) planes antiferrromagnetically [1]. Early paramagnetic-susceptibility measurements by Jonker [2] showed that the Curie constant does not change noticeably on heating across the first-order orbital order–disorder transition at $T_{JT} \approx 750$ K, but the Weiss constant θ increased abruptly from $\theta < T_N$ to $\theta > T_N$ thereby signalling 3D ferromagnetic interactions above T_{JT}. On the assumption that $LaMnO_3$ remains an insulator above T_{JT}, this observation led to the deduction that where the orbital ordering fluctuates, there is a *vibronic* 3D ferromagnetic superexchange interaction between Mn(III) spins across the bridging oxygen. However, a later measurement [3] of stoichiometric, single-crystal $LaMnO_3$ under vacuum showed that this compound becomes conductive with a thermoelectric power $\alpha(T) \approx 0$ above T_{JT}; thermal excitation of the reaction 2 Mn(III) = Mn(IV) + Mn(II) sets in above a $T^* \approx 600^\circ$C to create mobile holes and electrons within clusters in the orbitally ordered matrix, and the reaction is stabilized on a fraction of the Mn atoms above T_{JT}. This disproportionation reaction, which introduces a double-exchange component into the ferromagnetic interactions above T_{JT}, is made possible by breathing-mode bond-length fluctuations, and in the orbitally disordered phase above T_{JT} or within an orbitally disordered fluctuation within an orbitally ordered matrix in the interval $T^* < T < T_{JT}$, breathing-mode fluctuations coexist with orbital fluctuations at Mn(III) ions. The conductive phase is therefore *vibronic* with mobile charge carriers strongly coupled to the bond-length fluctuations. Electrons move diffusively, but without an activation energy. Tobe et al. [4] subsequently presented optical-conductivity data showing a closing of the energy gap at the Fermi energy on heating through T_{JT}, but they found no Drude component in the conductive phase, thus confirming the vibronic character of the mobile charge carriers. *"Bad-metal" behavior is typical of vibronic conduction due to the presence of bond-length fluctuations.*

The observation of vibronic conduction above T_{JT} suggested to us that the localized e electrons in $LaMnO_3$ are approaching the transition from localized to itinerant electronic behavior from the localized-electron side. Therefore, we undertook a study of the variation of the Néel temperature T_N with pressure to determine whether pressure reduces the splitting of the Mn(III)/Mn(II) and Mn(IV)/Mn(III) redox couples so as to break down the superexchange pertubation theory [5]. In order to clarify whether $LaMnO_3$ approaches crossover to itinerant e electrons, we turned to the empirical Bloch rule for the variation of T_N with volume V, viz.

$$a_B \equiv \mathrm{d}\log T_N / \mathrm{d}\log V \approx -3.3, \quad (4)$$

which Bloch has shown to be valid for a large number of antiferromagnetic oxides [6]. The theoretical justification for this rule is based on the superexchange expression

$$T_N \sim b^2 [U^{-1} + (2\Delta)^{-1}] \quad \text{with } b \approx |b^{ca}|^2/\Delta, \quad (5)$$

where b^{ca} is the Mn–O resonance integral for transfer of an electron from the O^{2-} ion to the Mn^{3+}/Mn^{2+} redox

couple across an energy gap Δ and U is the on-site electrostatic energy required to transfer an electron from one Mn(III) ion to another. The first term in Eq. (5) corresponds to the conventional Anderson superexchange, the second is the semicovalent exchange component [7, 8] associated with the transfer of two electrons from the same O-2p orbital, one to a Mn(III) on one side and the other to the Mn(III) on the opposite side of the O^{2-} ion. Theoretical calculations [9, 10] have given $b^{ca} \sim (M\text{–O})^{-n}$ with $n \approx 2.5$ and therefore $T_N \sim (M\text{–O})^{-10} \sim V^{-3.3}$ or $\alpha_B \approx -3.3$ if U and Δ are pressure independent.

Evaluation of α_B consists of measuring $T_N^{-1}\,dT_N/dP$ and the compressibility $V^{-1}dV/dP$. Our measurement yielded $\alpha_B \approx -3.0$ for $YCrO_3$, -3.8 for $CaMnO_3$ and, in the pressure range $7 < P < 20$ kbar, -5.3 for $LaMnO_3$ with evidence for a two-phase range near 7 kbar and perhaps also above 20 kbar at the end of the pressure range of the experiment. The breakdown of the Bloch rule in $LaMnO_3$ indicates that the assumption that U and/or Δ are independent of the bandwidth has broken down; as the transition to itinerant-electron behavior is approached, U and Δ are reduced by increased screening and band broadening as the equilibrium (M–O) bond length is reduced. Moreover, the appearance of a two-phase pressure range signals the transition from localized to itinerant electronic behavior may occur in two or more first-order steps in $LaMnO_3$.

2.2. $LaMn_{1-x}Ga_xO_3$

An early study [11] designed to test the deduction of vibronic 3D-ferromagnetic Mn(III)–O–Mn(III) superexchange interactions in the insulator system $LaMn_{1-x}Ga_xO_3$ confirmed this prediction. However, the O′-orthorhombic ($c/a < \sqrt{2}$) structure persisted throughout the range $0 \leqslant x \leqslant 0.5$, thereby signaling orbital order in zero applied magnetic field in at least a percolating matrix; and an orbitally ordered phase should be antiferromagnetic like $LaMnO_3$. In 1961, the concept of a spin glass had not yet been formulated. Therefore, we undertook a single-crystal reexamination of the system over the range $0 \leqslant x \leqslant 0.5$ [12]. This study showed the presence of a ferromagnetic, orbitally disordered phase coexisting with the antiferromagnetic, orbitally ordered phase. Where the Curie temperature of the ferromagnetic phase is $T_c < T_N$, the system is antiferromagnetic with no ferromagnetic ordering of isolated ferromagnetic inclusions; but in the range $0.3 \leqslant x \leqslant 0.5$, a $T_c > T_N$ produced a spin glass with a spin-freezing temperature T_f greater than the T_N extrapolated from T_N vs x with $x \leqslant 0.20$. However, in an applied magnetic field $H > 1$ kOe, the spin glass became ferromagnetic ($T_f \to T_c$) with a magnetization at 5 K of $4\,\mu_B$/Mn, the theoretical spin-only value. This experiment not only confirmed the existence of *a vibronic 3D-ferromagnetic* Mn(III)–O–Mn(III) *superexchange* associated with bond-length fluctuations at Mn(III) ions where the Jahn-Teller local distortions are disordered; it also demonstrated that in *a modest applied magnetic field, the orbitally disordered ferromagnetic phase grows at the expense of an antiferromagnetic, orbitally ordered matrix*.

3. Spin–lattice interactions

Bond-length fluctuations destroy phonons and magnons; they therefore suppress the phonon and magnon contributions to the thermal conductivity $\kappa(T)$. Fig. 1 shows, for example, the progressive suppression of $\kappa(T)$ below the magnetic ordering temperature in $LaMn_{1-x}Ga_xO_3$ by the presence of orbital fluctuations at Mn(III) ions. On the other hand, $\kappa(T)$ is also low above T_N in $LaMnO_3$ where the orbitals are ordered. Therefore, we measured $\kappa(T)$ for $CaMnO_3$ and found that in the paramagnetic range, it has an even lower $\kappa(T)$ than $LaMnO_3$ even though it contains no Jahn–Teller ion. In order to test whether this suppression is due to an exchange striction associated with the semicovalent component of the exchange interaction, we also investigated $\kappa(T)$ for $LaGaO_3$, $YCrO_3$ and $SmNiO_3$; the charge transfer gap Δ decreases on going from $YCrO_3$ to $LaMnO_3$ to $CaMnO_3$ to $SmNiO_3$, Fig. 2 [13]. The resulting $\kappa(T)$ and $\kappa^{-1}(T)$ curves were compared to those of $LaGaO_3$, Fig. 3. The Ga(III) ion carries no spin, and $LaGaO_3$ has a normal $\kappa(T)$; the antiferromagnetic compounds with comparable T_N values all show a suppression of $\kappa(T)$ above T_N that is larger where Δ is smaller. From this observation, we can conclude that the suppression of the phonon contribution to $\kappa(T)$ in these

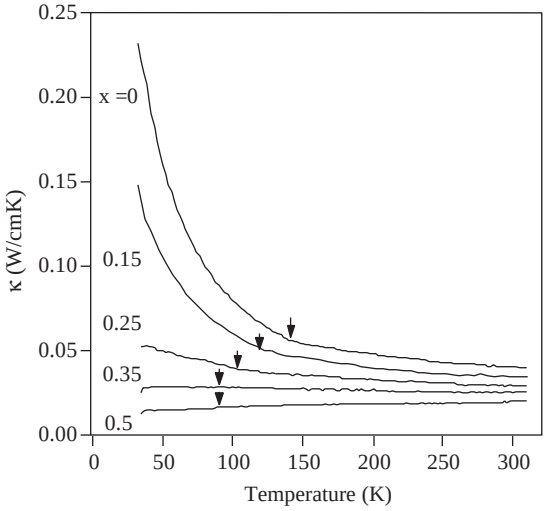

Fig. 1. Temperature dependence of the thermal conductivity κ for single-crystal samples of $LaMn_{1-x}Ga_xO_3$. The arrows mark T_N or T_f obtained from measurement of the magnetic susceptibility.

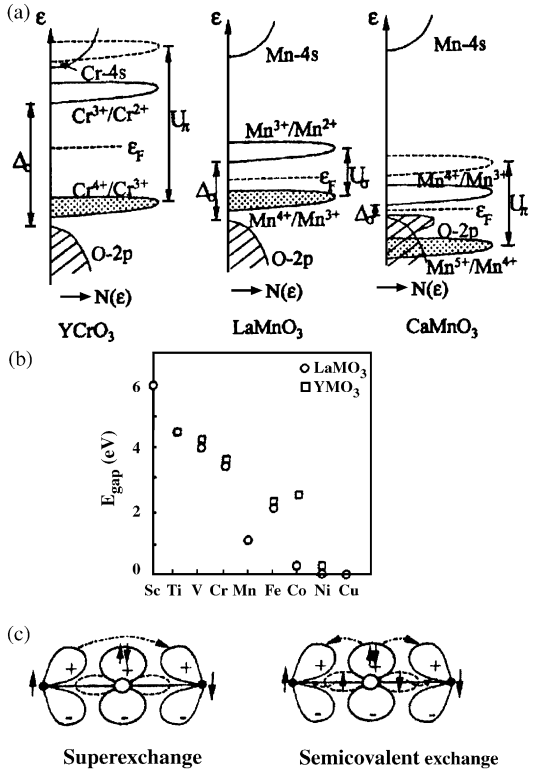

Fig 2. (a) Schematic energy diagrams for $YCrO_3$, $LaMnO_3$, and $CaMnO_3$. (b) The charge transfer gap Δ measured by optical spectra, after T. Arima, Y. Tokura, and J.B. Torrance, Phys. Rev. B 48 (1993) 17006. (c) Virtual electron transfers for 180° t^3e^0-O-t^3e^0 in Anderson superexchange and semicovalent exchange. In Anderson superexchange, the operative transfer integrals are between the crystal-field orbitals $\psi_t = N_\pi\,(f_t - \lambda_\pi \phi_\pi)$.

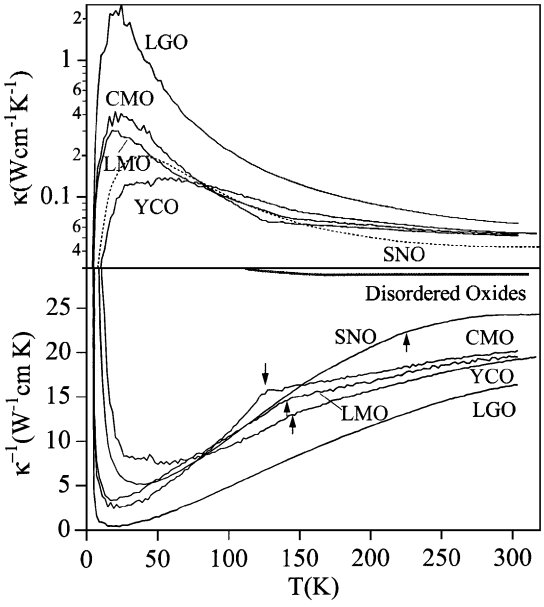

Fig. 3. Thermal conductivity $\kappa(T)$ and its inverse of single-crystal $LaGaO_3$ (LGO), $LaMnO_3$ (LMO), $CaMnO_3$ (CMO), and large-grained $YCrO_3$ (YCO), and $SmNiO_3$ (SNO). The dotted line is that of an oxide glass. The arrows indicate the Néel temperatures T_N.

electronic insulators is due to a bond-length fluctuation that is induced by a spin–lattice interaction occurring where the spins are disordered and that the strength of the spin–lattice coupling increases as Δ decreases. Anderson superexchange leaves the O^{2-} ion of an M–O–M interaction midway between the transition-metal ions M no matter the angle between their spins, but antiferromagnetic near neighbors shrinks the M–O–M bond. On the other hand, semicovalent exchange would shift an O^{2-} ion from the midpoint position where the spins on the M ions are not collinear. We therefore conclude that phonons are suppressed in a paramagnetic perovskite with localized spins on the MO_3 array by an exchange striction associated primarily with the semicovalent component of the exchange interaction. Moreover, from this experiment, *we may infer the presence of a semicovalent component of the spin–spin M–O–M exchange interaction.*

4. Crossover from localized to itinerant electrons

4.1. The single-valent $RNiO_3$ family

The RNiO$_3$ (R = rare-earth) family of perovskites offers the opportunity to study the crossover from localized to itinerant electronic behavior on the NiO_3 array with increasing size of the R^{3+} ion. The phase diagram is shown in Fig. 4. Rhombohedral, metallic $LaNiO_3$ contains low-spin Ni(III); the single electron per Ni(III) of e-orbital parentage occupies a narrow σ^* band, but a temperature dependence of the paramagnetic susceptibility signals that the transition from itinerant-σ^* to localized-e electronic behavior is approached from the itinerant-electron side. As the ionic radius of the R^{3+} ion is reduced, the σ^* band is

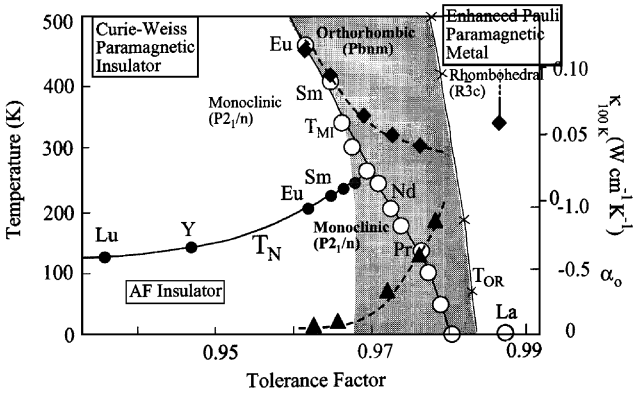

Fig. 4. Phase diagram of the $RNiO_3$ family. The shaded area is the two-phase region; stray correlation fluctuations are present in $LaNiO_3$. The diamond is for the lattice contribution of the thermal conductivity $\kappa(T)$ at 100 K; the circles are from J. B. Torrance et al., Phys. Rev. B 45, (1992) 820 and T_{OR} is from M. L. Medarde, J. Phys: Condens. Matter 9 (1997) 1679.

narrowed and antiferromagnetic order appears below an insulator–metal transition at $T_{IM} = T_N$ in $PrNiO_3$ and $NdNiO_3$. However, a $T_N < T_{IM}$ is found in $SmNiO_3$ and all the $RNiO_3$ perovskites with heavier rare-earth ions. The $RNiO_3$ perovskites exhibiting an insulator–metal transition are O-orthorhombic ($c/a > \sqrt{2}$) above T_{IM} and monoclinic with two distinguishable Ni sites below T_{IM} [14]. The neutron-diffraction data [15, 16] below T_N do not allow deduction of a unique magnetic order. However, a $T_N \propto \langle \cos^2\theta \rangle$, where $\theta = (180^\circ - \phi)$ is the Ni–O–Ni bond angle, satisfies the superexchange prediction for localized-electron configurations for all $RNiO_3$ perovskites with $T_N < T_{IM}$. On the other hand, $LaNiO_3$ has been found to approach the crossover from the itinerant-electron side [17–19]. Therefore, we have investigated how the physical properties change in the narrow range of tolerance factors on going from $SmNiO_3$ to $LaNiO_3$.

Since $SmNiO_3$ appears to approach the crossover from the localized electron side, we measured the Bloch parameter α_B for $SmNiO_3$; like $LaMnO_3$, it had an anomalously large $|\alpha_B| \approx 5.5$ and exhibited a two-phase region under applied hydrostatic pressure [20]. Moreover, a hydrostatic pressure of 14 kbar decreased the resistivity of $PrNiO_3$ at 15 K by five orders of magnitude while decreasing T_{IM} from near 150 K to about 80 K. Pressure increased the tolerance factor ($dt/dP > 0$), which shows that the (Ni–O) bond is unusually compressible, and the return under pressure of bad-metal behavior below T_{IM} demonstrates stabilization by pressure of a conductive phase coexisting with the insulator phase until it grows beyond percolation before T_{IM} falls to zero. The two-phase character was also manifest in the paramagnetic susceptibility $\chi(T)$ of $Nd_{0.5}Sm_{0.5}NiO_3$, which has $T_{IM} > T_N$; $\chi(T)$ did not change on cooling through T_{IM}, which demonstrated that the insulator–metal transition is not a global opening of an energy gap at the Fermi energy, but is rather an ordering of two fluctuating phases into a charge-density wave [21]. Given this evidence for two-phase fluctuations in the transitional compositions between $SmNiO_3$ and $LaNiO_3$, we undertook a study of the thermal conductivity [19].

In order to obtain reliable thermal conductivity data on polycrystalline samples, a cold-pressing technique was developed that gave hard ceramic samples of large enough grain size. Fig. 5 shows the thermal conductivity $\kappa(T)$ and its inverse for samples from $EuNiO_3$ to $LaNiO_3$. It was necessary to subtract out the electronic contribution $\kappa_e(T)$ as calculated from the Wiedemann–Franz law in the case of the conductive $RNiO_3$ samples with R = La, Pr, and Nd. From these data, it can be seen that the phonons are not strongly suppressed in $LaNiO_3$ or below T_N in the insulators $SmNiO_3$ and $EuNiO_3$; but $NdNiO_3$ and $PrNiO_3$ show a dramatic suppression of $\kappa(T)$ below $T_N = T_{IM}$. This suppression is still present,

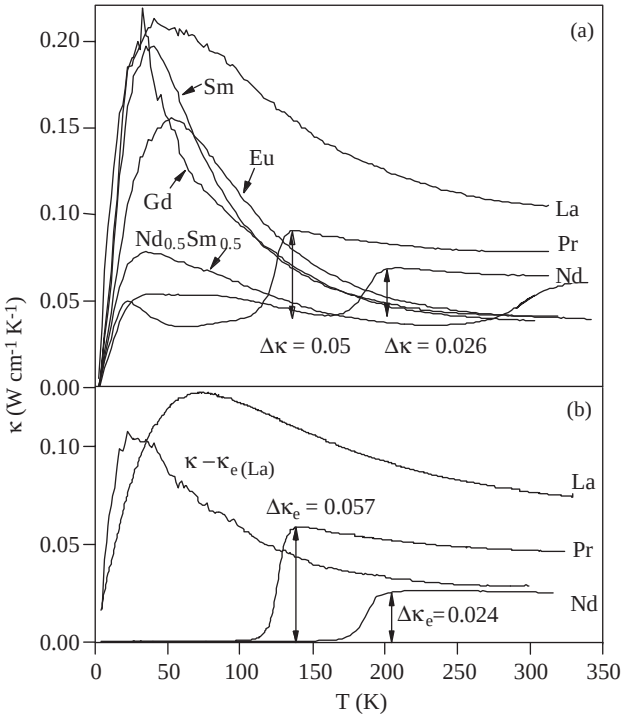

Fig. 5. (a) Temperature dependence of the thermal conductivity in the cold-pressed samples $RNiO_3$. (the rare-earth atom R is labeled on each curve). (b) The upper-bound electronic contribution to the thermal conductivity $\kappa_e(T)$ in cold-pressed $RNiO_3$ (R = La, Pr, and Nd) calculated from the resistivity in the corresponding samples via the Wiedemann–Franz law.

but to a lesser degree, in $Nd_{0.5}Sm_{0.5}NiO_3$. Fig. 4 shows how $\kappa(T)$ is progressively suppressed as T_{IM} decreases, the two-phase fluctuations giving a maximum suppression near the boundary between the orthorhombic and rhombohedral phases.

A localized e electron at a low-spin Ni(III) would induce Jahn–Teller distortions with attendant orbital fluctuations in the $RNiO_3$ family; however, the monoclinic distortion below T_{IM} suggests a disproportionation toward Ni(IV)O_6 molecular clusters and Ni(II): t^3e^2 localized configurations that increases on going from R = Sm to R = Y. The monoclinic distortion, which distinguishes two Ni sites, is also present below T_{IM} in $NdNiO_3$, but the two-phase character reduces sharply the apparent disproportionation. The resulting charge-density wave in the monoclinic phase may give superexchange coupling between localized configurations across a molecular-orbital cluster rather than uniform, localized Ni(III): t^6e^1 configurations undergoing a cooperative Jahn–Teller deformation.

4.2. A mixed-valent crossover in $R_{0.5}A_{0.5}MnO_3$

The $R_{0.5}A_{0.5}MnO_3$ perovskites with A = alkaline-earth have a fixed ratio Mn(IV)/Mn(III) = 1, but it is possible to pass from localized to itinerant electronic behavior on

the MnO_3 array by varying the mean size of the *A*-site cations and hence the geometric tolerance factor t. In this family, the evolution of the competing phases at the crossover tolerance factor t_c is made even more complex by the existence of charge as well as orbital ordering in the localized-electron phases and the formation of Mn(III)–O–Mn(IV) molecular clusters (Zener polarons) or orbital ordering of narrow σ^* bands in the itinerant-electron phases.

Several groups have presented temperature vs tolerance factor phase diagrams [22–27]. Kuwahara and Tokura [21] and Rivadulla et al. [23] had stoichiometric single-crystal data and were the only groups to recognize the existence of a critical tolerance factor t_c separating localized from itinerant electronic behavior; their two phase diagrams are shown in Fig. 6. Tokura et al. [24] were also the first to report the existence of a narrow, ferromagnetic metallic phase inserted between two antiferromagnetic Type-CE insulator phases that they identified as COI in their diagram. They made no distinction between the two COI phases as they assumed the Type-CE antiferromagnetic order necessarily implied a charge ordering as Mn(III) and Mn(IV) ions as well as a Jahn–Teller orbital ordering at the Mn(III) ions as originally predicted in 1955 [1]. Therefore, they considered the ferromagnetic phase to represent a metastable state appearing at a quantum critical point (QCP) where two-phase fluctuations suppress not only charge order (CO), but also orbital order (OO) and magnetic order. But such a critical point occurs at a crossover from localized to itinerant electronic behavior where the bond-length fluctuations are strongest, so the assumption that the two CE antiferromagnetic-insulator (AFI) phases either side of $t = t_c$ both contain CO may prove to be invalid. Our data [23] suggest that the classical CO phase occurs for $t > t_c$, but that an ordering of Zener polarons should be found with $t > t_c$. Quite independently, Daoud-Aladine et al. [28] have provided direct evidence of Zener-polaron ordering in a Type-CE antiferromagnetic phase with neutron diffraction in a $Pr_{0.6}Ca_{0.4}MnO_3$ crystal.

We have interpreted the phase diagram of Fig. 6(b), which was determined near $t = t_c$ with single-crystal data from the system $Pr_{0.5}(Ca_{1-x}Sr_x)_{0.5}MnO_3$ having a relatively small variance of the A-site cations, as follows [23]. Above T_{SP}, the paramagnetic susceptibility has Curie–Weiss behavior with a Weiss constant $\theta > 250$ K, which is indicative of ferromagnetic vibronic superexchange spin–spin interactions where there are orbital fluctuations as well as Zener double-exchange interactions. From the susceptibility and thermoelectric-power data, we could estimate the presence of about 20% two-Mn Zener polarons, and these introduce a superparamagnetic component to the paramagnetic susceptibility below T_{SP}.

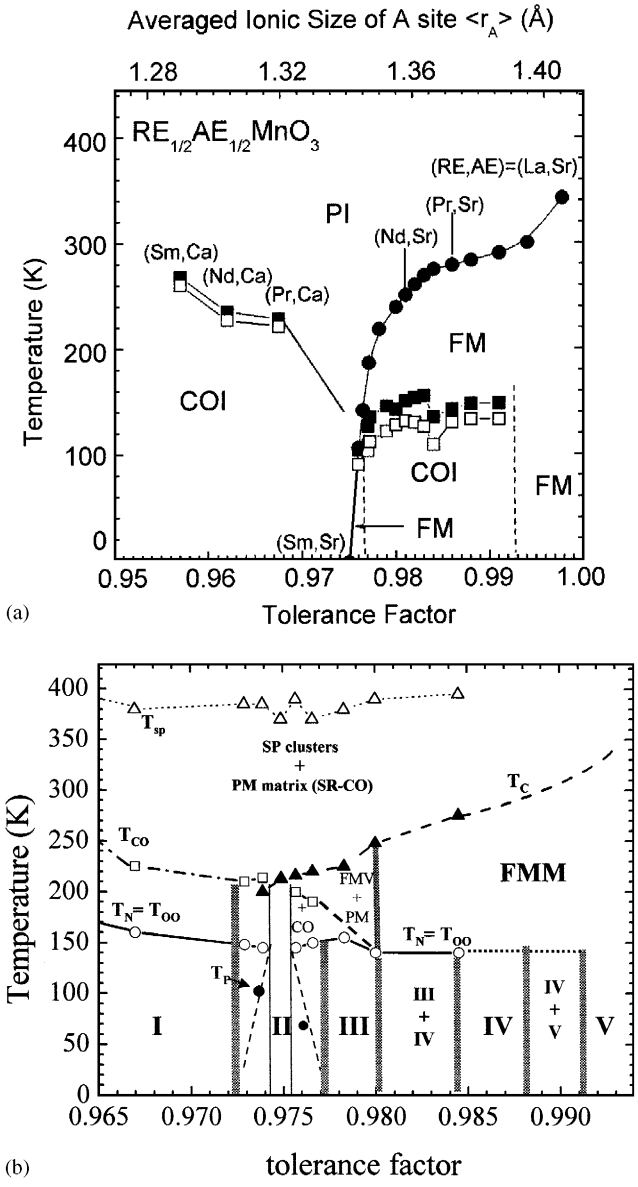

Fig. 6. Temperature vs tolerance factor phase diagrams for $R_{0.5}A_{0.5}MnO_3$ from (a) [21] and (b) [22]. In (a), PI = paramagnetic insulator, COI = charge-ordered insulator, FM = ferromagnetic metal. In (b), SP = superparamagnetic, SRCO = short-range charge-ordered fluctuations, I = localized CE antiferromagnetic insulator, II = ferromagnetic metal (FMM), FMV = ferromagnetic vibronic, PM = paramagnetic, III = Zener-polaron CE antiferromagnetic insulator, IV = Type-A antiferromagnetic metal (AFM), V = FMM; shaded boundaries are estimates.

The calculated tolerance factors of Fig. 6(b) are based on 12-fold coordination of the A-site cations; crossover occurs at a $t_c \approx 0.975$. On cooling samples with $t < 0.972$, a charge-ordering transition occurs at $T_{CO} \approx 225$ K; an orbital ordering is accompanied by the onset of Type-CE antiferromagnetic order below a $T_N = T_{OO} \approx 160$ K. In this phase I, a CO of Mn(III) and Mn(IV) breaks up the Zener pairs to stabilize localized electrons that order below T_N in the classical orbitally order CE AFI

configuration below $T_N = T_{OO}$. Samples with $t > 0.992$ are metallic ferromagnets (FMM) below T_c to lowest temperatures, phase V. Between phases I and V there is a transition from localized to itinerant electrons of e-orbital parentage.

The transition temperatures T_{CO} for the CO phase and T_c for an FM phase cross at $t = t_c$ where a unique FMM phase II appears. This phase is suppressed by small deviations from oxygen stoichiometry or where the variance of the sizes of A-site cations is larger; it was found to have a larger room-temperature volume than expected for a smooth evolution of volume with t, so it is also suppressed by the application of hydrostatic pressure. The larger volume, which we assume is stabilized by displacements of the A-site cations, straightens the Mn–O–Mn bond angle to give an effective tolerance factor $t_{eff} > 0.99$. Tokura's diagram shows that where phase II is suppressed, the bond-length fluctuations occurring at t_c suppress all ordering to give quantum-critical-point (QCP) behavior.

Between t_c and $t = 0.99$, two additional phases appear. Phase III appears as a Type CE AFI phase setting in below a Curie temperature T_c of a ferromagnetic, vibronic phase (FMV); this CE phase is predicted to be composed of ordered Zener polarons. Phase IV appears as a Type-A antiferromagnetic metallic phase setting in below T_c of a FMM phase; unlike the Type-A AFI phase of $LaMnO_3$, the A-AFM phase IV has metallic (001) planes as a result of ordering of the twofold-degenerate σ^* bands into an occupied $x^2-y^2\sigma^*$ band and an empty $3z^2-r^2\sigma^*$ band. In phase V, the twofold degeneracy of the σ^* bands is not removed by orbital ordering.

In the two-phase regions between phases, the ferromagnetic, conductive phases are stabilized by an applied magnetic field relative to the CO and OO phases, and large magnetoresistance effects are observed.

5. Conclusions

From this brief review of several single-valent and mixed-valent transition-metal oxides having the perovskite structure, the following general conclusions can be drawn for perovskite-related oxides containing $(180^\circ - \phi)$ M–O–M bonds between transition-metal atoms M.

1. Localized electrons at Jahn–Teller ions induce bond-length fluctuations above a cooperative orbital-ordering temperature; these fluctuations (a) introduce 3D-ferromagnetic vibronic superexchange interactions, (b) give "bad-metal' vibronic conductivity, and (c) allow disproportionation breathing-mode fluctuations. Consequently, an external magnetic field stabilizes an orbitally disordered ferromagnetic phase relative to an antiferromagnetic orbitally ordered phase in single-valent perovskites containing Mn(III) ions. In mixed-valent manganese-oxide perovskites, charge order accompanies orbital order, and an external magnetic field may disorder charge as well as orbital ordering to induce not only ferromagnetic order, but also a large resistance change.
2. In a single-valent system containing a Jahn–Teller ion, cooperative bond-length ordering may stabilize, at lower temperatures, either cooperative Jahn–Teller distortions of the $MO_{6/2}$ octahedra as in $LaMnO_3$ or cooperative disproportionations as in $YNiO_3$ into two distinguishable sites.
3. Spin–lattice interactions associated with the semicovalent component of the superexchange interactions may induce bond-length fluctuations in the paramagnetic state of charge-transfer oxides.
4. The crossover from localized to itinerant electronic behavior is first-order, and in oxoperovskites a spinodal phase segregation may be accomplished by cooperative oxygen displacements; these displacements may be dynamic giving rise to two-phase fluctuations of small length scale. The two fluctuating phases may either order into a charge-density wave or remain dynamic to suppress all long-range order and give QCP behavior.

Acknowledgments

The authors thank the NSF, the Robert A. Welch Foundation at Houston, TX, and the Texas Center for Superconductivity of the University of Houston (TCSUH) for financial support. Francisco Rivadulla thanks the Fulbright Foundation and the Ministry of Science of Spain for a post-doctoral fellowship.

References

[1] J.B. Goodenough, Phys. Rev. 100 (1955) 545.
[2] G.H. Jonker, Physica 22 (1956) 707.
[3] J.-S. Zhou, J.B. Goodenough, Phys. Rev. B 60 (1999) R15002.
[4] K. Tobe, T. Kimura, Y. Okimoto, Y. Tokura, Phys. Rev. B 64 (2001) 184421.
[5] J.-S. Zhou, J.B. Goodenough, Phys. Rev. Lett. 89 (2002) 87201.
[6] D. Bloch, J. Phys. Chem. Solids 27 (1966) 881.
[7] P.W. Anderson, Phys. Rev. 115 (1959) 2.
[8] J.B. Goodenough, Magnetism and the Chemical Bond, Interscience–Wiley, New York, 1963.
[9] K.N. Shrivastava, V. Jaccarino, Phys. Rev. B 13 (1976) 299.
[10] D.W. Smith, J. Chem. Phys. 50 (1969) 2784.
[11] J.B. Goodenough, A. Wold, R.J. Arnott, N. Menyuk, Phys. Rev. 124 (1961) 373.
[12] J.-S. Zhou, H.Q. Yin, J.B. Goodenough, Phys. Rev. B 63 (2001) 184423.
[13] J.-S. Zhou, J.B. Goodenough, Phys. Rev. B 66 (2002) 052401.

[14] J.A. Alonso, J.L. García-Muñoz, M.T. Fernández-Díaz, M.A.G. Aranda, M.J. Martínez-Lope, M.T. Casais, Phys. Rev. Lett. 82 (1999) 3871;
J.A. Alonso, J.L. García-Muñoz, M.T. Fernández-Díaz, M.A.G. Aranda, M.J. Martínez-Lope, M.T. Casais, Phys. Rev. B 61 (2000) 1756;
J.A. Alonso, J.L. García-Muñoz, M.T. Fernández-Díaz, M.A.G. Aranda, M.J. Martínez-Lope, M.T. Casais, Phys. Rev B 64 (2001) 094102.
[15] J.L. García-Muñoz, J. Rodriguez-Carvajal, P. Lacorre, Europhys. Lett. 20 (1992) 241.
[16] J. Rodríguez-Carvajal, S. Rosenkranz, M. Medarde, P. Lacorre, M.T. Fernández-Díaz, F. Fauth, V. Trounov, Phys. Rev. B 57 (1998) 456.
[17] I.H. Inoue, I. Hase, Y. Aiura, A. Fujimori, Y. Haruyama, T. Maruyama, Y. Nishihara, Phys. Rev. Lett. 74 (1995) 2539.
[18] J.-S. Zhou, J.B. Goodenough, Phys. Rev. B 54 (1996) 13393.
[19] J.-S. Zhou, J.B. Goodenough, B. Dabrowski, Phys. Rev. B 61 (2000) 4401.
[20] J.-S. Zhou, J.B. Goodenough, B. Dabrowski, Phys Rev. B 67 (2003) 020404(R).
[21] J.-S. Zhou, J.B. Goodenough, B. Dabrowski, P.W. Klamut, Z. Bukowski, Phys. Rev. Lett. 84 (2000) 520.
[22] H. Kuwahara, Y. Tokura, in: C.N.R. Rao, B. Raveau (Eds.), Colossal Magnetoresistance, Charge Ordering and Related Properties of Manganese Oxides, World Scientific, Singapore, 1998.
[23] F. Rivadulla, E. Winkler, J.-S. Zhou, J.B. Goodenough, Phys. Rev. B 66 (2002) 174432.
[24] Y. Tokura, H. Kuwahara, Y. Moritomo, Y. Tomioka, A. Asamitsu, Phys. Rev. Lett. 76 (1996) 3184.
[25] C.N.R. Rao, A. Arulraj, P.N. Santosh, A.K. Cheetham, Chem. Mater. 10 (1998) 2714.
[26] F. Damay, C. Martin, A. Maignan, M. Hervieu, B. Raveau, Z. Jirak, G. André, F. Bourée, Chem. Mater. 11 (1999) 536.
[27] S. Krupicka, M. Marysko, Z. Jirák, J. Hejtmánek, J. Magn. Magn. Mater. 206 (1999) 45.
[28] M. Daoud-Aladine, J. Rodrígíuez-Carvajal, L. Pinsard-Gaudart, M.T. Fernández-Díaz, A. Revcolevschi, Phys. Rev. Lett. 89 (2002) 097205.